DIFFERENCE COARRAY OF MULTI-FREQUENCY SPARSE RATIONAL ARRAYS

Md. Waqeeb T. S. Chowdhury[†], *Yimin D. Zhang*[†], *and Lu Gan*[‡]

[†] Department of Electrical and Computer Engineering, Temple University, USA
[‡] Department of Electrical and Electronic Engineering, Brunel University of London, UK

ABSTRACT

This paper investigates the difference coarray structure of multi-frequency sparse rational arrays and evaluates their direction-of-arrival (DOA) estimation performance in the coarray domain. The proposed approach reformulates the rational configuration into a spatially oversampled representation with reduced inter-element spacing, aligning it with an integer grid. This transformation eliminates fractional lags and thus facilitates a more structured analysis of the coarray properties. Furthermore, the proposed rational array generates more unique difference coarray lags than its integer-based counterpart, thereby enhancing signal identifiability. Through Cramér-Rao bound (CRB) analysis and simulations, we demonstrate that the rational sparse array achieves lower estimation error and resolves more signals for a given aperture compared to its integer-based counterpart, underscoring its effectiveness and robustness in high-resolution DOA estimation.

***Index Terms*—** Direction-of-arrival estimation, multi-frequency sparse array, rational sparse array, spatial oversampling, group sparsity.

1. INTRODUCTION

Optimized design of sparse linear arrays (SLAs) has attracted substantial research interest over the past few decades due to their ability to estimate the directions-of-arrival (DOAs) of $\mathcal{O}(N^2)$ signals using only N sensors [1–3]. In contrast to uniform linear arrays (ULAs) which are limited to resolving a maximum of $N-1$ signals, SLAs leverage difference coarrays to enhance the achievable degrees-of-freedom (DOFs) and improve signal identifiability. Several SLA configurations have been proposed with closed-form expressions for sensor locations, enabling systematic analysis of their coarray structures and achievable DOFs [4–14]. Recent advancements in array signal processing, including those based on compressive sensing and array interpolation, have further increased the number of achievable DOFs and enhanced DOA estimation performance [15, 16].

By leveraging the frequency-dependent nature of the array manifold, virtual coprime arrays can be synthesized using a single ULA excited by two continuous-wave signals with coprime frequency ratios [17]. This approach generalizes the spatial domain coprime array concept, originally formulated using two physical subarrays, to a joint spatio-spectral domain with a single physical array. Recent studies have extended this concept to multiple coprime frequencies and analyzed the resulting DOF improvements [18–21]. Multi-frequency sparse arrays can be implemented in a frequency-switching fashion for reduced system complexity [22]. Additionally, multi-frequency sparse rational array designs were explored to construct redundancy-free difference coarrays, maximizing the achievable DOFs for a given number of sensors [23]. More recently, multi-frequency sparse rational arrays have been introduced as a flexible alternative to integer-based multi-frequency arrays [24, 25]. Multi-frequency sparse rational arrays offer greater flexibility in sensor placement than sparse integer arrays, which are limited to integer multiples of half-wavelength spacing. However, their impact on difference coarray structures and DOA estimation in the coarray domain remains largely unexplored.

In this paper, we investigate the coarray properties of multi-frequency sparse rational arrays and highlight their advantages over integer-based designs. We reformulate these arrays as spatially oversampled virtual integer arrays, enabling a denser coarray structure with enhanced coarray lags. Our analysis shows that rational sparse arrays achieve a greater number of unique difference coarray lags than their integer-based counterparts, leading to improved signal identifiability. Additionally, we compare the Cramér-Rao bound (CRB) benchmark and present simulation results highlighting the enhanced signal identifiability and DOA estimation performance.

Notations: We use bold lowercase (uppercase) characters to denote vectors (matrices). In particular, $\mathbf{I}_N$ denotes the $N \times N$ identity matrix and $\mathbf{1}^N$ denotes an $N \times 1$ vector of ones. The transpose and Hermitian operations of a matrix or a vector are denoted by $(\cdot)^{\mathrm{T}}$ and $(\cdot)^{\mathrm{H}}$, respectively, whereas the vectorization of a matrix is denoted by $\mathrm{vec}(\cdot)$. The greatest common divisor (GCD) and the least common multiple (LCM) of two integers a and b are given by $\gcd(a,b)$ and $\mathrm{lcm}(a,b)$, respectively. The operator $\ominus$ computes the pairwise differences between all possible combinations of elements from the two sets, while $\otimes$ represents the Kronecker product. $\mathbb{E}[\cdot]$ stands for the statistical expectation operator, $||\cdot||_p$ denotes the ℓ_p norm, and $|\cdot|$ computes the absolute value. $\mathbb{C}^{M\times N}$ denotes the $M \times N$ complex space and $\mathbb{Z}^+$ is the set of positive integers.

2. SIGNAL MODEL

We consider a scenario where I continuous-wave signals with carrier frequencies f_i, for $i = 1, 2, \cdots, I$, are emitted from either a single transmit antenna or a phased array. The signals are reflected by L far-field targets and impinge on an N-element linear array with physical sensors at locations

$$\mathbb{P} = \{0 = p_1, p_2, \cdots, p_N\}d. \tag{1}$$

Let λ_i denote the wavelength corresponding to carrier frequency f_i. The element spacing d is expressed as $d = M_i\lambda_i/2$, where $M_i > 0$ can be either an integer (integer array) or a rational number (rational array). In the general case, we define M_i as a positive rational

The work of M. W. T. S. Chowdhury and Y. D. Zhang was supported in part by the National Science Foundation (NSF) under grant No. ECCS-2236023. L. Gan was partially supported by UK EPSRC grant EP/Z00084X/1.

number $M_i = a_i/b_i$ where $a_i, b_i \in \mathbb{Z}^+$, which becomes an integer when $b_i = 1$. In this case, the virtual array for the ith frequency is expressed as

$$\tilde{\mathbb{S}}_i = \{0, M_i p_2, \cdots, M_i p_N\} \frac{\lambda_i}{2}. \tag{2}$$

Denoting the DOA of the lth signal as θ_l, $l = 1, 2, \cdots, L$, the received signal $\tilde{\mathbf{x}}_i(t) \in \mathbb{C}^{N\times 1}$ associated with the ith frequency is given by

$$\tilde{\mathbf{x}}_i(t) = e^{\jmath 2\pi f_i t} \sum_{l=1}^{L} \rho_l^{(i)}(t) \mathbf{a}_i(\theta_l) + \tilde{\mathbf{n}}_i(t), \tag{3}$$

where $\rho_l^{(i)}(t)$ denotes the frequency-dependent reflection coefficient of the lth target,

$$\mathbf{a}_i(\theta_l) = \left[1,\ e^{-\jmath \frac{2\pi p_2 d}{\lambda_i} \sin(\theta_l)}, \cdots,\ e^{-\jmath \frac{2\pi p_N d}{\lambda_i} \sin(\theta_l)}\right]^{\mathrm{T}} \tag{4}$$

is the steering vector of the lth signal for the ith frequency, and $\tilde{\mathbf{n}}_i(t)$ denotes an additive white Gaussian noise vector, independent between different frequencies. The baseband signal vector after demodulation with carrier frequency f_i is given as

$$\mathbf{x}_i(t) = \sum_{l=1}^{L} \rho_l^{(i)}(t) \mathbf{a}_i(\theta_l) + \mathbf{n}_i(t) = \mathbf{A}_i \mathbf{s}_i(t) + \mathbf{n}_i(t), \tag{5}$$

where $\mathbf{A}_i = [\mathbf{a}_i(\theta_1),\ \mathbf{a}_i(\theta_2), \cdots, \mathbf{a}_i(\theta_L)] \in \mathbb{C}^{N\times L}$ is the array manifold matrix for the ith frequency, $\mathbf{s}_i(t) = [\rho_1^{(i)}(t), \rho_2^{(i)}(t), \cdots, \rho_L^{(i)}(t)]^{\mathrm{T}} \in \mathbb{C}^{L\times 1}$, and $\mathbf{n}_i(t) \sim \mathcal{CN}(0, \sigma_n^{(i)} \mathbf{I}_N)$ is the baseband additive white Gaussian noise vector. Let $\bar{d}$ denote the half-wavelength spacing in the normalized sense. We can rewrite (2) as

$$\mathbb{S}_i = \{0, M_i p_2, \cdots, M_i p_N\} \bar{d} = \left\{0, \frac{a_i}{b_i} p_2, \cdots, \frac{a_i}{b_i} p_N\right\} \bar{d}. \tag{6}$$

The multi-frequency sparse rational array corresponding to all I frequencies is given by

$$\mathbb{S} = \bigcup_{i=1}^{I} \mathbb{S}_i = \bigcup_{i=1}^{I} \left\{0, \frac{a_i}{b_i} p_2, \cdots, \frac{a_i}{b_i} p_N\right\} \bar{d}. \tag{7}$$

The number of virtual sensors in $\mathbb{S}$, denoted as N', satisfies $N' \leq (N-1)I + 1$, with equality holding when virtual sensors from the I frequencies overlap only at the reference position.

3. DIFFERENCE COARRAY ANALYSIS FOR MULTI-FREQUENCY SPARSE RATIONAL ARRAYS

3.1. Spatial Oversampling Representation of Multi-Frequency Sparse Rational Arrays

The GCD of any Q positive rational numbers $r_q = u_q/v_q$ with $u_q, v_q \in \mathbb{Z}^+$, $q = 1,\ 2, \cdots, Q$, is given by [26]

$$\gcd(r_1, r_2, \cdots, r_Q) = \frac{\gcd(u_1, u_2, \cdots, u_Q)}{\mathrm{lcm}(v_1, v_2, \cdots, v_Q)}. \tag{8}$$

Using the distributive and associative properties, the GCD of the sensor locations of the virtual array $\mathbb{S}$ in (7) becomes

$$\beta = \frac{\gcd(a_1, \cdots, a_I) \cdot \gcd(p_2, \cdots, p_N)}{\mathrm{lcm}(b_1, \cdots, b_I)}. \tag{9}$$

The sensor location $(a_i/b_i)p_n$ of the virtual array $\mathbb{S}_i$ in (6) can be re-written as

$$\frac{a_i}{b_i} p_n = \beta \cdot l_n^{(i)} \tag{10}$$

for $n = 1, 2, \cdots, N$, where $l_n^{(i)}$ indicates the scaled virtual sensor location for the ith frequency. Defining

$$\tilde{M}_i = \frac{a_i}{b_i \beta}, \tag{11}$$

$l_n^{(i)}$ can be written into

$$l_n^{(i)} = \tilde{M}_i p_n. \tag{12}$$

Noting in (9)–(11) that a_i is divisible by $\gcd(a_1, \cdots, a_I)$, p_n is divisible by $\gcd(p_2, \cdots, p_N)$, and $\mathrm{lcm}(b_1, \cdots, b_I)$ is divisible by b_i, we conclude that $\tilde{M}_i$ and, consequently, $l_n^{(i)}$ are positive integers. As a result, the sensor locations of the virtual array $\mathbb{S}_i$ in (6) can be reformulated as

$$\mathbb{S}_i = \{0, \tilde{M}_i p_2, \cdots, \tilde{M}_i p_N\} \tilde{d}, \tag{13}$$

where $\tilde{d} = \beta \bar{d}$ can be regarded as the unit inter-element spacing. Since $\tilde{M}_i \in \mathbb{Z}^+$ for $i = 1, \cdots, I$, $\mathbb{S}$ corresponding to all I frequencies consists of virtual sensors positioned at integer multiples of the reduced inter-element spacing $\tilde{d}$. It is noted that coprimality of the sensor locations was established as a necessary and sufficient condition for unambiguous DOA estimation in [27]. A set of rational numbers is considered coprime if the GCD of the set is less than or equal to one [26]. Therefore, it follows by definition that $\beta \leq 1$ and, equivalently, $\bar{d} \geq \tilde{d}$. It can be observed in (9) that $\bar{d} = \tilde{d}$ holds only when $M_i \in \mathbb{Z}^+$, i.e., $b_i = 1$, for all $i = 1, \cdots, I$. When $\bar{d} < \tilde{d}$, $\mathbb{S}$ becomes a spatially oversampled sparse array.

3.2. Lag Analysis

In the previous subsection, we reformulated multi-frequency sparse rational arrays as a spatially oversampled representation with a reduced inter-element spacing $\tilde{d}$, ensuring that all virtual sensor locations align with integer indices in the $\tilde{d}$-spaced grid. Such a reformulation simplifies the coarray analysis since the resulting difference lags are also aligned with the integer grid. The self-lags represent the coarray sensor positions obtained from differences between virtual sensors within the same frequency. For I frequencies, the self-lags are defined as

$$\mathbb{D}_{\mathrm{self}} = \bigcup_{i=1}^{I} \mathbb{S}_i \ominus \mathbb{S}_i. \tag{14}$$

Similarly, the cross-lags correspond to sensor location differences between virtual sensors associated with different frequency pairs $i \neq k \in \{1, 2, \cdots, I\}$ and are given as

$$\mathbb{D}_{\mathrm{cross}} = \bigcup_{i\neq k} \mathbb{S}_i \ominus \mathbb{S}_k. \tag{15}$$

The complete set of the difference coarray lags of the virtual array $\mathbb{S}$, denoted by $\mathbb{D} = \mathbb{D}_{\mathrm{self}} \cup \mathbb{D}_{\mathrm{cross}}$, is given as

$$\begin{aligned} \mathbb{D} &= \bigcup_{i,i'=1}^{I} \left\{\frac{a_i}{b_i} p_n - \frac{a_{i'}}{b_{i'}} p_m\right\} \bar{d} \\ &= \bigcup_{i,i'=1}^{I} \left\{\frac{a_i b_{i'} p_n - a_{i'} b_i p_m}{b_i b_{i'}}\right\} \bar{d}, \end{aligned} \tag{16}$$

where $n, m \in \{1, 2, \cdots, N\}$.

Redundancy-free sparse array was considered in [23] for multi-frequency integer sparse arrays, i.e., $b_i = b_{i'} = 1$, where the frequencies and the physical arrays are carefully designed to ensure all nonzero lags to be redundancy-free. Elimination of redundancy in the difference lags guarantees a high number of unique lags for enhanced DOA estimation performance. However, for integer sparse arrays, such designs often require large separation between the frequencies as well as the physical sensors. For the underlying multi-frequency sparse rational arrays, as we can flexibly select parameters b_i and $b_{i'}$ in (16), the increased dimension of parameters enables difference coarrays with a greater number of unique lags than integer-based counterparts. As a result, not only can redundancy-free arrays be designed with more practical selections of both frequencies and physical sensor locations, but we can also achieve a better lag profile with desirable missing entries.

3.3. Design Example

In this subsection, we present a simple example of a multi-frequency sparse rational array with $I = 2$ frequencies to demonstrate spatially oversampled representations. We consider an SLA with physical sensor locations

$$\mathbb{P} = \{0, 1, 2, 4\}d. \tag{17}$$

The two carrier frequencies f_1 and f_2 are chosen with ratios $M_1 = 1.8$ and $M_2 = 3$ such that $a_1 = 9, b_1 = 5, a_2 = 3$, and $b_2 = 1$. The virtual arrays corresponding to f_1 and f_2 are respectively given as

$$\mathbb{S}_1 = \left\{0, \frac{9}{5}, \frac{18}{5}, \frac{36}{5}\right\}\bar{d} \text{ and } \mathbb{S}_2 = \{0, 3, 6, 12\}\bar{d}. \tag{18}$$

The total virtual array is obtained as

$$\mathbb{S} = \mathbb{S}_1 \cup \mathbb{S}_2 = \left\{0, \frac{9}{5}, 3, \frac{18}{5}, 6, \frac{36}{5}, 12\right\}\bar{d}. \tag{19}$$

It can be seen from (19) that not all virtual sensors of $\mathbb{S}$ are on the integer grid of $\bar{d}$. The GCD of the sensor locations in (19) is obtained as $\beta = 0.6$. Taking out the GCD component, the virtual arrays $\mathbb{S}_1$ and $\mathbb{S}_2$ in (18) can be rewritten as

$$\mathbb{S}_1 = \{0, 3, 6, 12\}\tilde{d} \text{ and } \mathbb{S}_2 = \{0, 5, 10, 20\}\tilde{d}, \tag{20}$$

where $\tilde{d} = 0.6\bar{d}$. Note for this design that $\tilde{M}_1 = 3$ and $\tilde{M}_2 = 5$. The virtual array $\mathbb{S}$ in (19) can therefore be reformulated as

$$\mathbb{S} = \{0, 3, 5, 6, 10, 12, 20\}\tilde{d}, \tag{21}$$

and the set of its positive difference coarray lags is obtained as

$$\mathbb{D}_+ = \{0, 1, 2, 3, 4, 5, 6, 7, 8, 9, 10, 12, 14, 15, 17, 20\}\tilde{d}, \tag{22}$$

which comprises a high number of consecutive lags and few missing elements for convenient missing-data interpolation.

4. DOA ESTIMATION USING OVERSAMPLED SPARSE RATIONAL ARRAY

4.1. Covariance Matrices

The self-covariance matrix $\mathbf{R}_{ii} \in \mathbb{C}^{N\times N}$ of the data received by the virtual array corresponding to the ith frequency is given by

$$\mathbf{R}_{ii} = \mathbb{E}[\mathbf{x}_i(t)\mathbf{x}_i^{\mathrm{H}}(t)] = \mathbf{A}_i\mathbf{R}_s^{(ii)}\mathbf{A}_i^{\mathrm{H}} + \sigma_n^{(i)}\mathbf{I}_N, \tag{23}$$

for $i = 1, 2, \cdots, I$, where $\mathbf{R}_s^{(ii)} = \mathbb{E}[\mathbf{s}_i(t)\mathbf{s}_i^{\mathrm{H}}(t)] \in \mathbb{C}^{L\times L}$ is the covariance matrix of the reflected signal vector for frequency f_i. This matrix is diagonal with real-valued entries. The cross-covariance matrix of the received data corresponding to the ith and kth frequency for $i \neq k$ is obtained as

$$\mathbf{R}_{ik} = \mathbb{E}[\mathbf{x}_i(t)\mathbf{x}_k^{\mathrm{H}}(t)] = \mathbf{A}_i\mathbf{R}_s^{(ik)}\mathbf{A}_k^{\mathrm{H}}, \tag{24}$$

where $\mathbf{R}_s^{(ik)} = \mathbb{E}[\mathbf{s}_i(t)\mathbf{s}_k^{\mathrm{H}}(t)]$ is the cross covariance matrix of the reflected signal vectors for frequencies i and k. Since signal corresponding to different frequencies experience distinct reflection coefficients and propagation phase delays, the matrix $\mathbf{R}_s^{(ik)}$ is diagonal with complex entries. In practice, when perfect statistics is unavailable, the sample covariance matrices can be estimated using T snapshots as

$$\hat{\mathbf{R}}_{ii} = \frac{1}{T}\sum_{t=1}^{T}\mathbf{x}_i(t)\mathbf{x}_i^{\mathrm{H}}(t) \text{ and } \hat{\mathbf{R}}_{ik} = \frac{1}{T}\sum_{t=1}^{T}\mathbf{x}_i(t)\mathbf{x}_k^{\mathrm{H}}(t). \tag{25}$$

4.2. Effect of Spatial Oversampling on Identifiability

Now we analyze the effect of spatial oversampling of an antenna array on its identifiability. By defining the received signal vector of the virtual array $\mathbb{S}$ as

$$\mathbf{x}(t) = [\mathbf{x}_1(t), \mathbf{x}_2(t), \cdots, \mathbf{x}_I(t)]^{\mathrm{T}}, \tag{26}$$

its covariance matrix is given as $\mathbf{R}_x = \mathbb{E}[\mathbf{x}(t)\mathbf{x}^{\mathrm{H}}(t)] \in \mathbb{C}^{N'\times N'}$. The eigenvalues of $\mathbf{R}_x$ in descending order are given as $\gamma_1 \geq \gamma_2 \geq \cdots \geq \gamma_L \geq \gamma_{L+1} = \cdots = \gamma_{N'}$. The largest L eigenvalues pertain to the signal subspace while the remaining $N' - L$ eigenvalues belong to the noise subspace. It is well established that the array loses its DOFs when some of the signal subspace eigenvalues fall beyond a certain threshold and, subsequently, the covariance matrix loses its numerical rank [28–30]. Note that the oversampled representation of the virtual array $\mathbb{S}$ is equivalent to an integer array compressed by a factor of β, and the effect on the identifiability due to compression was examined in [29] through the rank-revealing QR-decomposition of the covariance matrix. If $\mathbf{R}_x$ has a numerical rank r and there exists a permutation matrix $\mathbf{\Pi}$ such that performing QR-factorization on $\mathbf{R}_x\mathbf{\Pi}$ yields

$$\mathbf{R}_x\mathbf{\Pi} = \mathbf{Q}\bar{\mathbf{R}} = \mathbf{Q}\begin{bmatrix}\bar{\mathbf{R}}^{(11)} & \bar{\mathbf{R}}^{(12)} \\ \mathbf{0} & \bar{\mathbf{R}}^{(22)}\end{bmatrix}, \tag{27}$$

and if $\gamma_{\min}(\bar{\mathbf{R}}^{(11)}) > ||\bar{\mathbf{R}}^{(22)}||_2$ such that $\mathbf{Q} \in \mathbb{C}^{N'\times N'}$ is an orthonormal matrix, $\bar{\mathbf{R}} \in \mathbb{C}^{N'\times N'}$ is an upper triangular matrix, $\bar{\mathbf{R}}^{(11)} \in \mathbb{C}^{r\times r}$ and $\bar{\mathbf{R}}^{(22)} \in \mathbb{C}^{(N'-r)\times(N'-r)}$, then (27) is said to be a rank-revealing QR factorization of $\mathbf{R}_x$. From the eigenvalue interlacing property [31], the spectral norm of $\bar{\mathbf{R}}^{(22)}$ is chosen as the threshold to evaluate the numerical rank of $\mathbf{R}_x$. It was demonstrated that, as the array is compressed, the smallest signal subspace eigenvalues drop below the threshold and DOFs are lost.

4.3. Group Sparsity-Based DOA Estimation

By vectorizing the covariance matrix $\mathbf{R}_{ik}$ we have

$$\mathbf{r}_{ik} = \mathrm{vec}(\mathbf{R}_{ik}) = \begin{cases}\tilde{\mathbf{A}}_{ii}\mathbf{b}_{ii} + \sigma_n^{(i)}\mathbf{i}_N, & i = k, \\ \tilde{\mathbf{A}}_{ik}\mathbf{b}_{ik}, & i \neq k,\end{cases} \tag{28}$$

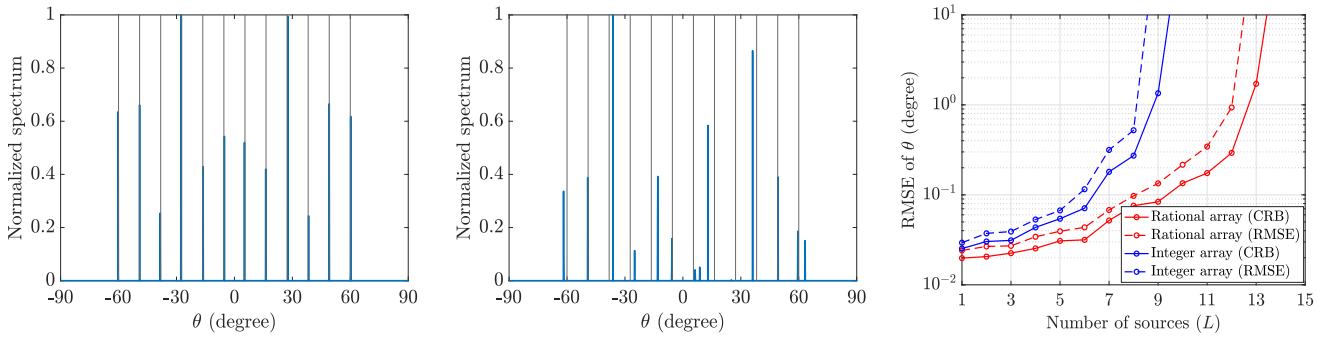

(a) Multi-frequency sparse rational array (b) Multi-frequency sparse integer array (c) CRB and RMSE vs. number of signals

Fig. 1: Comparison of multi-frequency sparse rational and integer arrays with group Lasso-based DOA spectra and CRB and RMSE versus number of sources (SNR = 5 dB, $T = 5{,}000$).

where $\tilde{\mathbf{A}}_{ik} = [\tilde{\mathbf{a}}_{ik}(\theta_1), \cdots, \tilde{\mathbf{a}}_{ik}(\theta_L)]$ with $\tilde{\mathbf{a}}_{ik}(\theta_l) = \mathbf{a}_i^*(\theta_l) \otimes \mathbf{a}_k(\theta_l)$, $\mathbf{b}_{ik} = \text{vec}(\mathbf{R}_s^{(ik)})$, and $\mathbf{i}_N = \text{vec}(\mathbf{I}_N)$. Here, $\tilde{\mathbf{A}}_{ik}$ is a virtual manifold corresponding to the augmented array with virtual sensors obtained from difference lag set $\mathbb{S}_i \ominus \mathbb{S}_k$. To employ group Lasso, we define I^2 optimization vectors $\mathbf{b}_{ik}$ of size $G \times 1$, where G is the number of grids across the DOA search space. The dictionary matrix for the G-point search grid corresponding to $\tilde{\mathbf{A}}_{ik}$ is given as $\mathbf{D}_{ik}$. Defining $\mathbf{B} = [\mathbf{b}_{11}, \cdots, \mathbf{b}_{1I}, \mathbf{b}_{21}, \cdots, \mathbf{b}_{ik}, \cdots, \mathbf{b}_{II}] \in \mathbb{C}^{G \times I^2}$, the group Lasso problem is formulated as [32]

$$\hat{\mathbf{B}} = \arg\min_{\mathbf{B}} \sum_{i=1}^{I} \sum_{k=1}^{I} ||\mathbf{r}_{ik} - \mathbf{D}_{ik}\mathbf{b}_{ik}||_2^2 + \eta ||\mathbf{b}_{ik}||_{1,2}, \tag{29}$$

where η is the regularization parameter and $||\cdot||_{1,2}$ is the $\ell_{1,2}$ norm. The estimated DOA vector across the G search grids is

$$\hat{\mathbf{b}} = \frac{|\hat{\mathbf{B}}| \cdot \mathbf{1}^{I^2}}{\max\left(|\hat{\mathbf{B}}| \cdot \mathbf{1}^{I^2}\right)}. \tag{30}$$

5. SIMULATION RESULTS

In this section, we provide simulation results that demonstrate the DOA estimation performance of multi-frequency sparse rational arrays and compare it with the multi-frequency integer array counterpart of an equal aperture.

We consider the physical array $\mathbb{P}$ as defined in (17). For the rational array, we adopt the design outlined in Section III where $I = 2$ carrier frequencies are selected such that $M_1 = 1.8$ and $M_2 = 3$. In contrast, for the integer counterpart, the two frequencies are chosen such that $M_1' = 2$ and $M_2' = 3$. This ensures that both arrays share the same aperture size, thereby allowing a fair comparison of their coarray properties. The sensor locations of the virtual array corresponding to the two frequencies are respectively

$$\mathbb{S}_1' = \{0, 2, 4, 8\}\bar{d} \text{ and } \mathbb{S}_2' = \{0, 3, 6, 12\}\bar{d}, \tag{31}$$

and the total integer virtual array from the two frequencies is

$$\mathbb{S}' = \{0, 2, 3, 4, 6, 8, 12\}\bar{d}. \tag{32}$$

The set of positive difference coarray lags of the virtual sensors in $\mathbb{S}'$ is given as

$$\mathbb{D}_+' = \{0, 1, 2, 3, 4, 5, 6, 8, 9, 10, 12\}\bar{d}. \tag{33}$$

It is noted that, due to the restrictive selection of parameters M_1' and M_2' in this case, $\mathbb{D}_+'$ contains less unique lags as compared to $\mathbb{D}_+$.

Fig. 1(a) and Fig. 1(b) show the DOA spectra for $L = 12$ uncorrelated signals uniformly distributed within the angular range $[-60°, 60°]$. The input signal-to-noise ratio (SNR) is 5 dB, and $T = 5,000$ snapshots are used. Since there are seven virtual sensors for both the rational and integer arrays as defined in (21) and (32), the problem setup corresponds to an underdetermined DOA estimation scenario. The DOA search grid is set to $0.01°$, and the regularization parameter is chosen as $\eta = 20$. It can be observed that the multi-frequency sparse rational array successfully resolves all 12 sources, whereas the integer array fails to resolve several signals due to its limited coarray structure.

Fig. 1(c) presents the CRB and the root mean square error (RMSE) performance of multi-frequency sparse rational and integer arrays as the number of sources increases. The rational array achieves significantly better CRB performance, particularly in high-source scenarios, owing to its larger set of unique lags, which improves identifiability. The RMSE results further validate this advantage; the integer array exhibits rapidly increasing estimation errors as the number of sources grows, while the rational array maintains a lower RMSE. The RMSE is obtained by averaging over 100 independent Monte Carlo trials. These results confirm that the rational array's enhanced coarray structure enables accurate resolution of more sources with reduced estimation error, making it a robust choice for high-resolution DOA estimation. Overall, the simulations confirm that multi-frequency rational arrays offer enhanced identifiability and robustness compared to their integer counterparts.

6. CONCLUSION

This paper presented a multi-frequency sparse rational array framework that leverages rational frequency ratios to achieve a spatially oversampled virtual array. By restructuring the virtual array onto a refined integer grid with reduced inter-element spacing, the proposed approach increases the number of coarray lags, enhancing identifiability and robustness in DOA estimation. Theoretical analysis and simulations demonstrated that the rational array outperforms its integer counterpart, offering a richer coarray structure with more unique lags. This enables the detection of more signals while maintaining lower RMSE, as confirmed by CRB analysis. The results underscore the superior identifiability and resolution of the rational array, particularly when the number of signals is high.

7. REFERENCES

[1] A. Moffet, "Minimum-redundancy linear arrays," *IEEE Trans. Antennas Propagat.*, vol. 16, no. 2, pp. 172–175, 1968.

[2] R. T. Hoctor and S. A. Kassam, "The unifying role of the coarray in aperture synthesis for coherent and incoherent imaging," *Proc. IEEE*, vol. 78, no. 4, pp. 735–752, 1990.

[3] H. Krim and M. Viberg, "Two decades of array signal processing research: The parametric approach," *IEEE Signal Process. Mag.*, vol. 13, no. 4, pp. 67–94, 1996.

[4] P. Pal and P. P. Vaidyanathan, "Nested arrays: A novel approach to array processing with enhanced degrees of freedom," *IEEE Trans. Signal Process.*, vol. 58, no. 8, pp. 4167–4181, 2010.

[5] P. P. Vaidyanathan and P. Pal, "Sparse sensing with coprime arrays," in *Proc. Asilomar Conf. Signals Syst. Comput.*, Pacific Grove, CA, 2010, pp. 1405–1409.

[6] P. Pal and P. Vaidyanathan, "Nested arrays in two dimensions, Part II: Application in two dimensional array processing," *IEEE Trans. Signal Process.*, vol. 60, no. 9, pp. 4706–4718, 2012.

[7] K. Han and A. Nehorai, "Nested array processing for distributed sources," *IEEE Signal Process. Lett.*, vol. 21, no. 9, pp. 1111–1114, 2014.

[8] S. Qin, Y. D. Zhang, and M. G. Amin, "Generalized coprime array configurations for direction-of-arrival estimation," *IEEE Trans. Signal Process.*, vol. 63, no. 6, pp. 1377–1390, 2015.

[9] Y. Liu and J. R. Buck, "High-resolution direction-of-arrival estimation in SNR and snapshot challenged scenarios using multi-frequency coprime arrays," in *Proc. Int. Conf. Acoust. Speech Signal Process. (ICASSP)*, New Orleans, LA, 2017, pp. 3434–3438.

[10] J. Liu, Y. Zhang, Y. Lu, S. Ren, and S. Cao, "Augmented nested arrays with enhanced DOF and reduced mutual coupling," *IEEE Trans. Signal Process.*, vol. 65, no. 21, pp. 5549–5563, 2017.

[11] Z. Zheng, W.-Q. Wang, Y. Kong, and Y. D. Zhang, "MISC array: A new sparse array design achieving increased degrees of freedom and reduced mutual coupling effect," *IEEE Trans. Signal Process.*, vol. 67, no. 7, pp. 1728–1741, 2019.

[12] A. Raza, W. Liu, and Q. Shen, "Thinned coprime array for second-order difference co-array generation with reduced mutual coupling," *IEEE Trans. Signal Process.*, vol. 67, no. 8, pp. 2052–2065, 2019.

[13] A. Ahmed and Y. D. Zhang, "Generalized non-redundant sparse array designs," *IEEE Trans. Signal Process.*, vol. 69, pp. 4580–4594, 2021.

[14] S. Sun and Y. D. Zhang, "4D automotive radar sensing for autonomous vehicles: A sparsity-oriented approach," *IEEE J. Sel. Topics Signal Process.*, vol. 15, no. 4, pp. 879–891, 2021.

[15] C. Zhou, Y. Gu, X. Fan, Z. Shi, G. Mao, and Y. D. Zhang, "Direction-of-arrival estimation for coprime array via virtual array interpolation," *IEEE Trans. Signal Process.*, vol. 66, no. 22, pp. 5956–5971, 2018.

[16] S. Liu, Z. Mao, Y. D. Zhang, and Y. Huang, "Rank minimization-based Toeplitz reconstruction for DOA estimation using coprime array," *IEEE Commun. Lett.*, vol. 25, no. 7, pp. 2265–2269, 2021.

[17] Y. D. Zhang, M. G. Amin, F. Ahmad, and B. Himed, "DOA estimation using a sparse uniform linear array with two CW signals of co-prime frequencies," in *Proc. IEEE Int. Workshop Computat. Adv. Multi-Sensor Adapt. Process. (CAMSAP)*, St. Martin, France, 2013, pp. 404–407.

[18] S. Qin, Y. D. Zhang, and M. G. Amin, "DOA estimation exploiting coprime frequencies," in *Proc. SPIE Wireless Sens. Localization Process. IX*, vol. 9103, 2014, pp. 105–111.

[19] S. Qin, Y. D. Zhang, M. G. Amin, and B. Himed, "DOA estimation exploiting a uniform linear array with multiple coprime frequencies," *Signal Process.*, vol. 130, pp. 37–46, 2017.

[20] M. Guo, Y. D. Zhang, and T. Chen, "Performance analysis for uniform linear arrays exploiting two coprime frequencies," *IEEE Signal Process. Lett.*, vol. 25, no. 6, pp. 838–842, 2018.

[21] A. Liu, X. Zhang, Q. Yang, and W. Deng, "Fast DOA estimation algorithms for sparse uniform linear array with multiple integer frequencies," *IEEE Access*, vol. 6, pp. 29 952–29 965, 2018.

[22] Y. D. Zhang and M. W. T. S. Chowdhury, "Frequency-switching sparse arrays," in *Proc. IEEE Sensor Array and Multich. Signal Process. Workshop (SAM)*, Corvallis, OR, 2024, pp. 1–5.

[23] S. Zhang, A. Ahmed, Y. D. Zhang, and S. Sun, "Enhanced DOA estimation exploiting multi-frequency sparse array," *IEEE Trans. Signal Process.*, vol. 69, pp. 5935–5946, 2021.

[24] Y. D. Zhang and M. G. Amin, "Multi-frequency rational sparse array for direction-of-arrival estimation," in *Proc. Int. Symp. Signals Circ. Syst. (ISSCS)*, Iasi, Romania, 2023, pp. 1–4.

[25] M. W. T. S. Chowdhury and Y. D. Zhang, "Unambiguous DOA estimation using multi-frequency rational sparse arrays," in *Proc. Asilomar Conf. Signals Syst. Comput.*, Pacific Grove, CA, 2023, pp. 1324–1328.

[26] P. Kulkarni and P. Vaidyanathan, "Non-integer arrays for array signal processing," *IEEE Trans. Signal Process.*, vol. 70, pp. 5457–5472, 2022.

[27] P. Vaidyanathan and P. Pal, "Direct-MUSIC on sparse arrays," in *Proc. Int. Conf. Signal Process. and Commun. (SPCOM)*, Bangalore, India, 2012, pp. 1–5.

[28] S. Ubaru, Y. Saad, and A.-K. Seghouane, "Fast estimation of approximate matrix ranks using spectral densities," *Neural Comput.*, vol. 29, no. 5, pp. 1317–1351, 2017.

[29] M. W. T. S. Chowdhury, Y. D. Zhang, W. Liu, and M. S. Greco, "Identifiability analysis of sensor arrays with sensors off half-wavelength grid," in *Proc. Int. Conf. Acoust. Speech Signal Process. (ICASSP)*, Seoul, Korea, 2024, pp. 8496–8500.

[30] M. W. T. S. Chowdhury and Y. D. Zhang, "Direction-of-arrival estimation exploiting oversampled uniform linear arrays," *IEEE Signal Process. Lett.*, vol. 33, pp. 51–55, 2026.

[31] W. H. Haemers, "Interlacing eigenvalues and graphs," *Linear Algebra Appl.*, vol. 226, pp. 593–616, 1995.

[32] A. Ahmed, D. Silage, and Y. D. Zhang, "High-resolution target sensing using multi-frequency sparse array," in *Proc. IEEE Sensor Array and Multich. Signal Process. Workshop (SAM)*, Hangzhou, China, 2020, pp. 1–5.